EasyChair Preprint

№ 629

Application of PSO-LSSVM in Bias Correction of Shipborne Anemometer Measurement

Tong Hu, Suiping Qi, Zhijin Qiu, Jing Zou and Dongming Wang

November 12, 2018

Application of PSO-LSSVM in Bias Correction of Shipborne Anemometer Measurement

Tong Hu, Suiping Qi, Zhijin Qiu, Jing Zou, and Dongming Wang

Institute of Oceanographic Instrumentation, Qilu University of Technology (Shandong Academy of Sciences), Qingdao 266001, China
tong.hu@hotmail.com

Abstract. Wind measurement from shipborne anemometer is susceptible to the airflow distortion due to ship hull and superstructure. The measurement bias needs to be minimized with regard to various meteorological and navigation applications. To address this problem, this study illustrates the feasibility to correct the measurement bias due to airflow distortion by applying Least Squares Support Vector Machine with Particle Swarm Optimization (PSO-LSSVM) method. The airflow field around hull and superstructure of an experimental ship is simulated by computational fluid dynamics (CFD) techniques. And then the nonlinear relationship between the airflow through conventional anemometer mounting sites on the main mast and the airflow through the reference point above bridge is implicitly obtained using the PSO-LSSVM regression. The dataset of relative wind observation taken during a sea trial is used to validate the effectiveness of this method. The results show that the established model efficiently eliminates most of the speed bias and reduces half of the direction bias of the mean relative wind, which indicates this method could be extended to estimate the undisturbed freestream on the open sea surface.

Keywords: Ship Airflow Field, Wind Measurement, CFD, PSO, LSSVM.

1 Introduction

Sea surface wind plays a primary role in the air-sea momentum, heat and water vapor exchange process. The field measurements of sea surface wind are mostly obtained from conventional observation platforms such as ships, buoys and offshore stations. As one data source of most marine meteorological field observations, ship platform provides long-term and continuous sea surface wind datasets. The shipborne anemometer measures the relative wind, and the true wind is calculated by the relative wind, ship speed and course. The data bias existed in the relative wind measurement is usually due to inherent characteristics of wind measurement from a moving platform of bluff-body, which leads to the necessary consideration about the airflow distortion as well as platform motion.

The airflow through the anemometer mounting site is distorted by the ship hull and superstructure, and makes the relative wind speed and direction measurements different from the undistorted freestream on the open sea surface. The measurement bias of

the relative wind speed and direction deviates the calculation result of the true wind speed and direction, which further affects the calculation of the sea surface friction velocity u_* and the drag coefficient C_{D10N}. For example, if the freestream speed is 10m/s, 10% wind speed bias will result in 27% bias of the momentum flux estimation [1].

The problem of wind measurement bias due to airflow distortion on ship platforms has been concerned for decades. Such measurement bias cannot be reduced by improving the accuracy of anemometers. The World Meteorological Organization suggests that the shipborne anemometer should be mounted on well-exposed positon close to the front edge of the installation surface and of a certain height [2]. However, the anemometer cannot be mounted far enough away from ship hull and superstructure, and thus it is more appropriate to correct the measurement bias by post processing.

With the development of CFD techniques, the airflow distortion around ship hull and superstructure can be analyzed more conveniently, which facilitates the relevant research. Yelland et al. showed that the bias of wind speed measurements did not vary within the range of 5~25m/s [3]. This opinion is consistent with the suggestion of Moat et al. that the airflow field around ship was insensitive to the Reynolds number in the range of 2×10^5~1×10^7 [4, 5]. Popinet et al. showed that the mean wind speed bias depended on the upwind angle rather than the Reynolds number [6]. Griessbaum et al. presented that the wind measurement bias would lead to 30~50% deviation of the gas transport rate k_g [7]. O'Sullivan et al. suggested that more CFD simulations with different upwind angles were necessary for wind measurement bias correction [8]. Wnęk et al. verified the consistency of the CFD simulation results and the experimental data for LNG vessels on wind loads [9].

This study presents an application to correct the relative wind measurement bias using the Least Square Support Vector Machines with Particle Swarm Optimization (PSO-LSSVM). In Section 2, we review the basic LSSVM formulation as well as the hyper-parameter selection based on PSO. Several issues associated with the modeling process, including CFD simulation and PSO-LSSVM modeling, are discussed in detail in Section 3. In Section 4, experimental results are presented to illustrate the effectiveness of the bias correction model. Conclusions are drawn in Section 5.

2 PSO-LSSVM Regression

The LSSVM proposed by Suykens and Vandewalle [10] has been extensively applied to nonlinear regression and system modeling [11, 12, 13]. The algorithm complexity of LSSVM is reduced greatly by solving linear algebraic instead of the computationally hard quadratic programming problem in the standard SVM. The nonlinear regression problem can be written as:

$$\begin{cases} \min J\left(w,\xi\right)=\dfrac{1}{2}w^Tw+\dfrac{1}{2}\gamma\sum_{i=1}^{n}\xi_i^2 \\ s.t.\quad y_i=w^T\varphi(x_i)+b+\xi_i \end{cases} \tag{1}$$

The Lagrange multiplier is introduced to solve the above equality-constrained optimization problem:

$$L(w,b,\xi,\alpha) = J\left(w,\xi\right) - \sum_{i=1}^{N} \alpha_i [w^T \varphi(x_i) + b + \xi_i - y_i] \tag{2}$$

The conditions for optimality are given by:

$$\begin{cases} w = \sum_{i=1}^{N} \alpha_i \varphi\left(x_i\right) \\ \sum_{i=1}^{N} \alpha_i = 0 \\ \alpha_i = \gamma \xi_i \\ w^T \varphi\left(x_i\right) + b + \xi_i - y_i = 0 \end{cases} \tag{3}$$

After eliminating w and ξ_i, one gets the following linear system:

$$\begin{bmatrix} 0 & 1_v^T \\ 1_v & \Omega + \gamma^{-1} I \end{bmatrix} \begin{bmatrix} b \\ \alpha \end{bmatrix} = \begin{bmatrix} 0 \\ y \end{bmatrix} \tag{4}$$

with:

$$\begin{cases} y = \left[y_1, y_2, \cdots, y_N\right]^T \\ 1_v = \left[1,1,\cdots,1\right]^T \\ \alpha = \left[\alpha_1, \alpha_2, \cdots, \alpha_n\right]^T \\ \Omega_{i,j} = K\left(x_i, x_j\right) \end{cases} \tag{5}$$

Eq. (4) can be solved for the parameters α_i and b by the least squares method. Therefore, the resulting model for nonlinear regression becomes:

$$y = f\left(x\right) = \sum_{i=1}^{N} \alpha_i K\left(x, x_i\right) + b \tag{6}$$

The PSO algorithm as an optimization technique introduced by Eberhart and Kennedy well simulates the social behavior of groups such as birds randomly looking for food [14]. In PSO, each single solution is taken as a particle in the search space. All of the particles have fitness values which are evaluated by fitness function. According to the fitness values, the particles move towards better solution areas by changing the velocity and location as follow:

$$\begin{cases} v_i\left(t+1\right) = w_0 v_i\left(t\right) + c_1 r_1 \left(p_{best} - x_i\right) + c_2 r_2 \left(g_{best} - x_i\right) \\ x_i\left(t+1\right) = x_i + v_i\left(t+1\right) \end{cases} \tag{7}$$

where x_i, v_i are the location and velocity of the i th particle, w_0 is the symbol for inertial weight, c_1 and c_2 represent learning rates which are positive constants, r_1 and r_2

describe two random numbers between zero and one, p_{best} is the best previous position recorded by the i th particle, and g_{best} is the best global position among the entire particles throughout searching history.

In solving the hyper-parameter selection of LSSVM including the kernel parameter and regularization parameter, each particle is requested to represent a potential solution, namely hyper-parameters combination [15]. In this study, the LSSVM with radial basis function (RBF) kernel is trained to model the wind measurement bias, and thus each particle in PSO represents candidate values of regularization parameter γ and kernel parameter σ. To define the fitness value, five-fold cross validations with training dataset for each particle and the mean squared error (MSE) is taken as the fitness value. The bias correction modeling based on PSO-LSSVM is described in Section 3.2.

3 Bias Correction Modeling

The distorted airflow at the anemometer mounting site under different conditions of freestream velocity and upwind angle are obtained by CFD simulations. Then the nonlinear relationship between the distorted airflow and the undistorted freestream is modeled by means of the PSO-LSSVM.

3.1 CFD Simulation

In this study, an experimental ship is taken as an example to research on bias correction method of shipborne anemometer measurement. The dimension of the computational domain is 6L(length)×6L(width)×1.6L(height) where L is the length of the ship. As illustrated in Fig.1, the ship is placed at the center of the bottom surface of the computational domain, and rotated in each CFD simulation case to achieve different upwind angles (0~360 ° at 10 ° intervals). The impact of ship swing is not considered in this study.

To simulate the relative wind measurement process onboard, the freestream entered from the inlet of the computational domain flows past the ship hull and superstructure. The velocity of freestream at the inlet is set with a logarithmic profile.

$$u = (u_* / k_v)\ln(z / z_0) \tag{8}$$

Wind speed at the height of 10 meters above sea level u_{10N} is set as 5m/s, 10m/s and 20m/s respectively in CFD simulation cases of the same upwind angle. The Kalman constant k_v is set as 0.4, and the roughness length z_0 is set as 2mm.

To capture the boundary layers effects along the walls of the ship model, a tetrahedral mesh of 2×10^6 elements with 5 prismatic layers on the model's surface is generated (Fig.2). The first layer thickness is proportional to the wall distance y+, which is close to 30. Similar to the wind tunnel test, the no-slip condition is specified on the

ship hull, superstructure and the walls of the computational domain. At the outlet zero pressure condition was imposed.

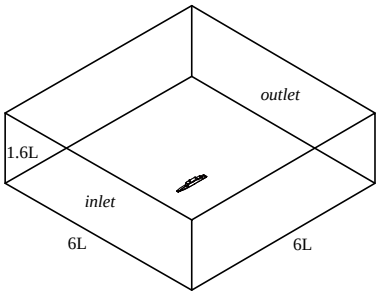

Fig. 1. Dimension of the computation domain

The turbulence closure scheme selected is *RNG* k-ε two-equation model which has been extensively used in industrial applications. The convection term is discretized using the second-order upwind scheme, and the diffusion term is discretized using the central difference scheme. Each solution was obtained by applying *SIMPLE* algorithm to solve the steady three-dimensional incompressible *RANS* equations. The convergence residual is set as 10E-4.

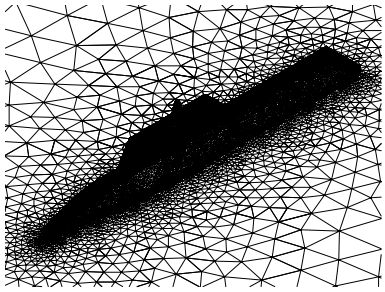

Fig. 2. Computational mesh

The speed and direction of the airflow through different wind measurement points on the experimental ship are extracted from the CFD simulation results. Besides the conventional wind measurement points on the both sides of the main mast, an additional anemometer used as reference was installed temporarily above the bridge during a sea trial.

In order to validate the CFD simulation results, the ratio of wind speed measured by the anemometers on the mast and the reference anemometer above the bridge is quantified under different upwind angles (Fig.3). The ratio calculated from CFD simulation results is consistent with the average value calculated from the experimental dataset. Since the airflow mainly comes from the bow during ship voyage, no measurement presents in certain upwind angles.

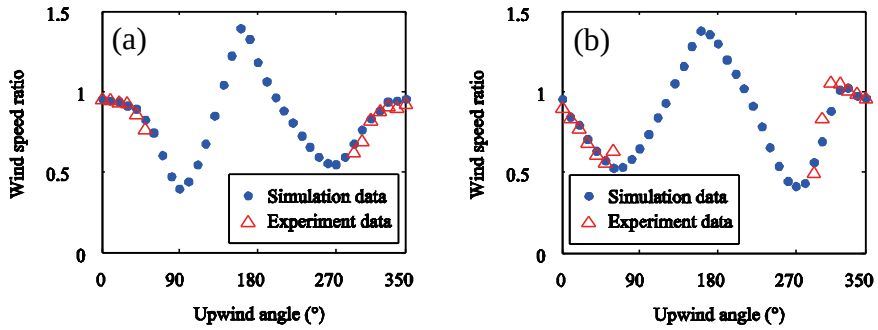

Fig. 3. Comparison of the wind speed ratios from CFD results and experimental dataset at the measurement site on the (a) port side and (b) starboard side

3.2 PSO-LSSVM Modeling

Since that it is difficult to carry out simultaneous field measurement of the undistorted sea surface wind, the relationship between the airflow through conventional anemometer mounting sites on the main mast and the airflow through the reference point above bridge is obtained based on PSO-LSSVM modeling, although the airflow through the reference measurement point will also be affected by the presence of the ship hull and superstructure. If the method could effectively reduce the wind measurement bias with respect to the reference measurement point, it could be applied to estimate the undisturbed freestream on the open sea surface by replacing the variables of airflow speed and direction taken from the reference measurement site with the one taken from the inlet of the computational domain.

The flowchart of the PSO-LSSVM modeling is shown in Fig. 4. Compared to the airflow speed, the direction of the airflow through measurement site on the main mast is relatively less affected by the ship hull and superstructure. Thus the direction of the airflow through measurement site on the main mast is selected as the input variable.

The output variables are the ratio of the airflow speed through measurement site on the main mast to the airflow speed through the reference measurement site above the bridge, as well as the direction difference between the airflow through measurement sites on the main mast and the airflow through the reference measurement site above the bridge.

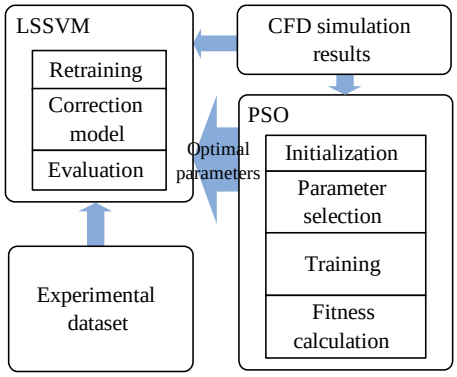

Fig. 4. Schematic diagram of the wind-bias correction

The relationship between the input and output variables is implicitly obtained using LSSVM regression with RBF kernel. The optimal hyper-parameter selection is solved by PSO, in which particles represents candidate values of regularization parameter γ and kernel parameter σ. The particle number is 30. The maximum number of iterations is 100. And the inertial weight w_0, learning rates c_1 and c_2 for the PSO algorithm are set as 0.9, 1.5, 1.5 respectively.

$$\begin{cases} f\left(wd_{mast}^{i}\right)=\left(r^{i},\Delta\theta^{i}\right) \\ r^{i}=ws_{mast}^{i}/ws_{bridge} \\ \Delta\theta^{i}=wd_{mast}^{i}-wd_{bridge} \end{cases} \quad i=starboard,port \tag{9}$$

where wd_{mast}^{i} is the direction of the airflow through the measurement site on the main mast, r^{i} is the ratio of the airflow speed through the measurement site on the main mast to the airflow speed through the reference measurement site, and $\Delta\theta^{i}$ is the direction difference between the airflow through measurement site on the main mast and the airflow through the reference measurement site above the bridge.

To reduce the wind measurement bias, the relative wind speed and direction are corrected according to corresponding r^{i} and $\Delta\theta^{i}$, then the corrected relative wind measurements from both sides on the main mast are merged by vector averaging.

4 Results And Discussion

In order to validate the effectiveness of the established bias correction model, the relative wind measurements from corresponding sites on the experimental ship were collected during a sea trial. The relative wind was measured at the frequency of 1Hz and move averaged with time window of 120s. The measurements from the anemometers installed on both sides of the main mast were input to the model respectively, then the outputs from the model were merged by vector averaging, and finally the

result was compared to the measurement from the reference anemometer above the bridge.

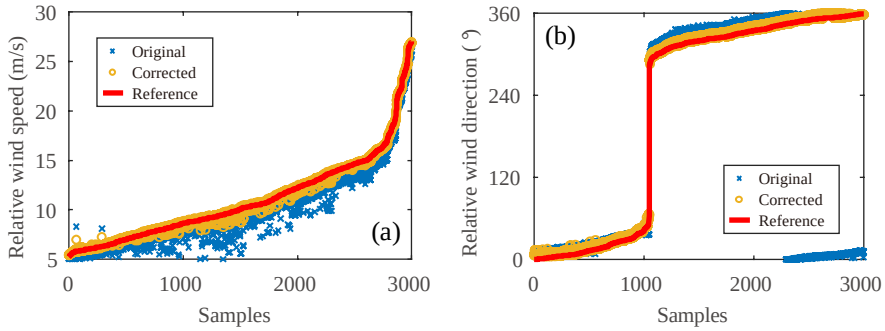

Fig. 5. Correction effects on (a) relative wind speed and (b) relative wind direction

In the sample data, the mean relative wind speed on the main mast is 92% on average of the one above the bridge. It indicates that the wind speed bias is about one tenth of the referenced mean relative wind speed. The direction difference of the mean relative wind between the measurements on the main mast and above the bridge is 13.4 °. As shown in Fig. 5, after correction by the established model, the wind measurements by the anemometer installed on the main mast are closer to the measurements by the anemometer installed above the bridge, which illustrates that relationship between the airflow through different wind measurement sites is well estimated by the PSO-LSSVM regression.

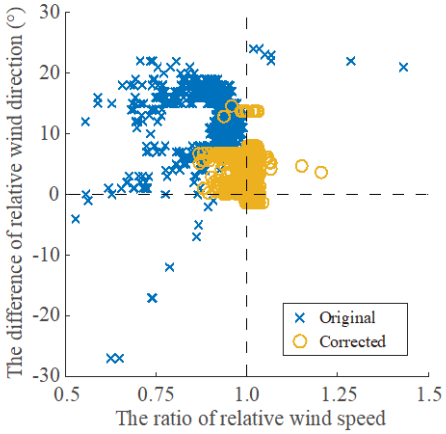

Fig. 6. Scatter plot of corrected wind speed ratio vs. direction difference

The scatter plot (Fig. 6) illustrates the ratio of the mean relative wind speed and the difference of the mean relative wind direction before and after the bias correction.

The Root Mean Square (RMS) of the ratio of the mean relative wind speed r was improved from 0.92 to 1.01, and meanwhile the RMS of the difference of the mean relative wind direction $\Delta\theta$ was reduced from 13.4 ° to 6.8 °.

It should be noted that the correction effect is not satisfactory for measurements of certain wind speed and direction. One of the possible causes is the differences between the CFD simulations and the actual environment conditions of the experimental ship at sea including the atmospheric turbulence and the sea state. It would benefit the accuracy of the established model if different wind speed profiles and turbulence settings under finer upwind angle intervals are considered.

5 CONCLUSION

The PSO-LSSVM method is applied to address the problem of wind measurement bias due to airflow distortion caused by the presence of the ship hull and superstructure. The empirical results demonstrated that the implicit relationship between airflow through different wind measurement sites implicitly obtained by PSO-LSSVM modeling using CFD simulation is consistent with the one in the experimental data. The established model eliminates most of the wind speed bias of the mean relative wind speed, and the direction bias of the mean relative wind measurements was reduced by half. Considering the operability to measure the undistorted sea surface wind during sea trial, the airflow through the measurement site above the bridge was selected as reference. To estimate the undisturbed freestream on the open sea surface, the referenced airflow would be replaced with the airflow at the inlet of the computational domain. It is required to validate the established model with the simultaneous field measurements of the undisturbed sea surface wind. Moreover, the atmospheric stability and sea state is not considered in CFD simulations. The effects of wind bias correction in more complicated conditions will be investigated in future work.

Acknowledgement. The study was supported by the Natural Science Foundation of China under Grant 41606112 and 41705046.

REFERENCES

1. Moat, B. I., Yelland, M. J., Pascal, R. W., Molland, A. F.: An overview of the airflow distortion at anemometer sites on ships. International Journal of Climatology 25(7), 997-1006 (2005).
2. World Meteorological Organization: Guide to meteorological instruments and methods of observation. 7th edn. World Meteorological Organization, Geneva, Switzerland (2008).
3. Yelland, M. J., Moat, B. I., Pascal, R. W., Berry, D. I.: Cfd model estimates of the airflow distortion over research ships and the impact on momentum flux measurements. Journal of Atmospheric & Oceanic Technology 19(10), 1477-1499 (2002).
4. Moat, B. I., Yelland, M. J., Pascal, R. W., Molland, A. F.: Quantifying the airflow distortion over merchant ships. part i: validation of a cfd model. Journal of Atmospheric & Oceanic Technology 23(3), 341-350 (2006).

5. Moat, B. I., Yelland, M. J., Molland, A. F.: Quantifying the airflow distortion over merchant ships. part ii: application of the model results. Journal of Atmospheric & Oceanic Technology 23(3), 351-360 (2006).
6. Popinet, S.: Experimental and numerical study of the turbulence characteristics of airflow around a research vessel. Journal of Atmospheric & Oceanic Technology 21(10), 1575-1589 (2004).
7. Griessbaum, F., Moat, B. I., Narita, Y., Yelland, M. J.: Uncertainties in wind speed dependent co2 transfer velocities due to airflow distortion at anemometer sites on ships. Atmospheric Chemistry and Physics 10(11), 5123-5133 (2010).
8. O'Sullivan, N., Landwehr, S., Ward, B.: Air-flow distortion and wave interactions on research vessels: an experimental and numerical comparison. Methods in Oceanography 12, 1-17 (2015).
9. Wnęk, A. D., Guedes Soares, C.: Cfd assessment of the wind loads on an lng carrier and floating platform models. Ocean Engineering 97, 30-36 (2015).
10. Suykens, J. A. K., Vandewalle, J.: Least squares support vector machine classifiers. Neural Processing Letters 9(3), 293-300 (1999).
11. Mellit, A., Pavan, A. M., Benghanem, M.: Least squares support vector machine for short-term prediction of meteorological time series. Theoretical. & Applied Climatology 111(1-2), 297-307 (2011).
12. Samui, P.: Application of Least Square Support Vector Machine (LSSVM) for Determination of Evaporation Losses in Reservoirs. Engineering 3(4), 431-434 (2011).
13. Wang, Q., Qian, W., He, K.: Unsteady aerodynamic modeling at high angles of attack using support vector machines. Chinese Journal of Aeronautics 28(3), 659-668 (2015).
14. Kennedy, J., Eberhart, R.: Particle swarm optimization. In: International Conference on Neural Networks, pp.1942-1948. IEEE Press, Perth, Australia.
15. Guo, X. C., Yang, J. H., Wu, C. G., Wang, C.Y., Liang, Y. C.: A novel LS-SVMs hyper-parameter selection based on particle swarm optimization. Neurocomputing 71(16-18), 3211-3215 (2008).